

Topological spin corner charge in the presence of spin-orbit coupling

Ran Gladstein Gladstone,¹ Minwoo Jung,² and Gennady Shvets¹

¹*School of applied and engineering physics, Cornell University**

²*Department of physics, Cornell University*

(Dated: March 1, 2025)

We investigate several C_6 second order topological insulators that are independently topological or trivial for two different spins, or pseudo-spins, using tight binding models and first principles electromagnetic simulations in the presence of spin orbit coupling (SOC). When the insulator is second order topological for both spins the corner charge is quantized to 0 and a topological phase transition can occur due to SOC. However, when the insulator is second order topological for only one of the spins, the corner charge is quantized to 1/2 and no topological transition can manifest.

The interplay of spin and topology has long been of interest to physicists [1–6]. Shortly after Chern insulators [1] had been discovered, researchers have extended the same idea to a system possessing spin 1/2 electrons, predicting the spin Hall effect [7] and leading to an extensive amount of results [8, 9]. The extension to spin 1/2 systems is usually intuitive and involves a doubling of the Hilbert space to include the subspaces for spin up and spin down electrons, resulting in two similar copies of the original spinless system [7, 10], but can have a significant effect on the topology of the system. For example, while the Chern insulator has a \mathbb{Z} topological invariant, a spin Chern insulator possesses a \mathbb{Z}_2 topological invariant due to time-reversal and inversion symmetries [11]. The addition of spin to the system has therefore changed its topological classification.

More recently, physicists have extended the concept of topological insulators to higher order topological insulators (HOTIs) [12–14], and their photonic counterparts (PHOTIs) [15–18], which are d dimensional topological insulator with a bulk topological invariant predicting topological states localized on some of its $d - n$ dimensional terminations, where $n \in \mathbb{N}$ and $d \geq n \geq 2$. A natural question to ask is whether the addition of spin to a HOTI maintains its topological properties, changes its topological classification or holds any other interesting effects that may not manifest with spinless HOTIs. In this letter we begin to answer that question for a specific class of HOTIs. While our work does not provide a general classification of spinful HOTIs, it introduces the first examples of the effects of the addition of spin to HOTIs, thereby encouraging further investigation and classification of these intriguing models. We note that our analysis applies not only to a spin degree of freedom (DOF), but also to other pseudo-spin DOFs such as layer [19–22] and polarization [23–25].

We inspect several different 2D lattice models and periodic electromagnetic waveguides possessing C_6 symmetry (rotation by 60°). For spinless models, these topological crystalline insulators have been shown to support a HOTI phase with a quantized corner charge of 1/2 [26]. When adding an independent subspace representing an

additional spin, an additional charge of 1/2 for the new spin species may appear. However, this does not have to be the case. One can judiciously choose the parameters of the new subspace, that do not have to be identical to the first, such that the additional subspace is a trivial topological phase, thus supporting no topological corner mode for the additional spin. This leads to four topologically distinct phases: a phase that is topological for both spins, a phase that is trivial for both spins and two hybrid phases that are topological for one of the spins but not the other. It is therefore natural to define a spin corner charge, in an analogy to the way the spin Chern number is defined [2, 3, 27], such that each spin has its own associated corner charge.

The addition of spin orbit coupling (SOC) [2] further enriches the physics displayed by these novel topological phases. We show that Kane-Mele SOC has no effect on the corner modes of the two hybrid phases, but can cause a topological phase transition to a quantum spin Hall (QSH) phase when applied to the phase that is topological for both spins. We define a new topological invariant, which is the sum of the spin polarized corner charges, and a new bulk quantity, the spin density weighted corner charge and use them to distinguish between the different topological phases. Below, we formalize these concepts, provide lattice models calculations, as well as first principles electromagnetic realizations of these novel HOTIs.

We begin by introducing the tight binding model we will realize in a photonic platform. Our model is a honeycomb lattice endowed with a Kekulé texture [16, 28], spin and SOC [1, 2]:

$$\begin{aligned}
 H = & \sum_{\langle ij \rangle} t_{\text{in}}^\dagger c_{i\uparrow}^\dagger c_{j\uparrow} + \sum_{\langle i'j' \rangle} t_{\text{out}}^\dagger c_{i'\uparrow}^\dagger c_{j'\uparrow} + \sum_{\langle ij \rangle} t_{\text{in}}^\dagger c_{i\downarrow}^\dagger c_{j\downarrow} \\
 & + \sum_{\langle i'j' \rangle} t_{\text{out}}^\dagger c_{i'\downarrow}^\dagger c_{j'\downarrow} + \sum_{\langle \langle ij \rangle \rangle_{\alpha\beta}} \frac{i}{3\sqrt{3}} \lambda_{\text{SOC}} \nu_{ij} s_{\alpha\beta}^z c_{i\alpha}^\dagger c_{j\beta},
 \end{aligned} \tag{1}$$

where the first (third) term describes the nearest neighbor intra unit cell hoppings of the spin up (down) electrons, the second (fourth) term describes the nearest neighbor inter unit cell hoppings of the spin up (down) electrons, and the fifth term describes the usual next

nearest neighbor Kane-Mele SOC [2]. when SOC is neglected, each spin subspace is independent of the other and, for each spin separately, it has been shown that this model accurately predicts a topological band inversion [16, 28] leading to a HOTI when $t_{\text{in}}^{\uparrow,\downarrow} < t_{\text{out}}^{\uparrow,\downarrow}$, or a trivial insulator otherwise. Since our model allows for independent control of the different hopping amplitudes, we find four different phases instead of two. The first is phase that is topological for both spins simultaneously. Another is phase that is trivial for both, and the third and fourth are hybrid phases that are topological for one of the spins but not the other. Naturally, one can then define a spin corner charge $Q_c^{\uparrow,\downarrow}$ as the corner charge [26] projected on each spin subspace respectively, in a similar fashion to how the spin Chern number is defined [7].

When SOC is added, one can show (see supplementary) that for the topological and trivial phases, when the hopping amplitudes of both spin subspaces are identical, the momentum space Hamiltonian is block diagonal. This block diagonal form is inaccessible for the hybrid phases since the hopping amplitudes cannot be equal for the two spin subspaces. This means that for the topological and trivial phases the spin corner charges $Q_c^{\uparrow,\downarrow}$ are well defined and are topological invariants that are robust to SOC. However, for the hybrid phases $Q_c^{\uparrow,\downarrow}$ are not well defined. We can define a total corner charge as $Q_c = (Q_c^\uparrow + Q_c^\downarrow)|_{\lambda_{\text{SOC}}=0}$, the sum of the spin polarized corner charges when SOC is neglected. This quantity is conserved even when SOC is added, since total corner charge is defined according to symmetry eigenvalues of the C_2 and C_3 operators of the energy bands at high symmetry points [26], and SOC maintains those symmetries (see supplementary). This quantity is then simply the usual Q_c defined by Benalcazar et al. [26] when all bands below the band gap are considered together, regardless of their spin density. However, the total corner charge fails to distinguish between the two different hybrid phases since both have $Q_c = 1/2 \pmod{1}$.

We therefore need to define an additional bulk quantity, the spin density weighted corner charge. We weigh each of these eigenvalues by the spin density of its mode $\langle S_z \rangle$ so that

$$[M] = \sum_i \langle S_z \rangle_i^M - \sum_i \langle S_z \rangle_i^\Gamma, \quad (2)$$

where the summation is done on all bands below the band gap with eigenvalue $+1$ to C_2 denoted by i , the first term sums the spin densities at the M point and the second at the Γ point. The spin density weighted corner charge is then defined as $S_c = [M]/4$. When SOC is neglected, this quantity becomes the difference between spin polarized corner charges of the different spins and is a topological invariant distinguishing the hybrid phases. This quantity is not conserved in the presence of SOC since for the calculation of S_c we need to distinguish between spin densities of the different bands, while for Q_c it is

unnecessary.

For convenience, we define $\Delta_{\uparrow,\downarrow} = t_{\text{out}}^{\uparrow,\downarrow} - t_{\text{in}}^{\uparrow,\downarrow}$ as the difference between inter cell and intra cell hopping amplitudes. While S_c is not strictly conserved for the hybrid phases, as can be seen by the color map of Fig.1, it retains values very close to the expected $\pm 1/2$, that distinguish the two hybrid phases, until the SOC strength is several times $\Delta_{\uparrow,\downarrow}$. We compare the bulk calculation of S_c to a calculation using corner local density of states (LDOS) [14] in Fig.1(c) and notice they maintain values very close to each other until very high SOC is considered. Our bulk definition of S_c using Eq.(2) is therefore useful for estimating the experimental signature of a spin polarized corner LDOS deficit. When $\lambda_{\text{SOC}}^2 = \Delta_\uparrow \Delta_\downarrow$ the bulk band gap closes and a phase transition occurs to a quantum spin Hall (QSH) phase. We can summarize all of the information regarding the different phases in a phase diagram shown in Fig.1.

The Hamiltonian of Eq.(1) conceptually resembles the Hamiltonian introduced by Ezawa [29]. Although they have completely different symmetries, realizing Eq.(1) in a physical system should allow access to the emulation of 2D magnetic HOTIs due to the presence of two spins and terms that introduce coupling between them. To realize the Hamiltonian of Eq.(1) in a physical system we use a platform of photonic crystal (PhC) waveguide made of perfect electric conductors (PEC) elements sandwiched between PEC plates [23–25], shown in Fig.2(a). The PhC possesses C_6 symmetry, thereby allowing a Kekulé distortion [30], which opens a band gap at the Γ point of the Brillouin Zone. Realizations of the hybrid phases of Eq.(1) are shown in Fig.2(b) and (c). When setting the gaps between the PEC elements and plates, $g_{\text{top}} = g_{\text{bot}}$ possesses mid-plane mirror symmetry $z \rightarrow -z$. When this is the case, the PhC's electromagnetic modes can be classified as either TE-like or TM-like, which are orthogonal to each other [31]. The TE-like modes are distinguished by having a non-vanishing H_z component at the $z = h/2$ plane while the TM-like modes have a non-vanishing E_z component, as shown in Fig.2(d).

For similar PhCs supporting a single polarization it has been shown that the modes below and above the band gap at the Γ point have profiles that correspond to p_x, p_y and $d_{xy}, d_{x^2-y^2}$ orbitals [16, 32]. When the bands below the band gap possess p orbital profile, the PhC has an orbital Chern number of $C_{\text{orb}} = 0$ [28], where the traditional role of the spin DOF is taken by the orbital DOF, and a corner charge of $Q_c = 0 \pmod{1}$ [26]. Changing the parameters of the PhC can cause a band inversion, switching the orbital profiles of the bands below and above the band gap, such that the bands below possess d orbital profiles [16, 28, 32]. When such a band inversion occurs, the orbital Chern number switches to $C_{\text{orb}} = 1$ and corner charge of $Q_c = 1/2 \pmod{1}$ [26] and the PhC is predicted to have two band gap spanning topological edge states, according to the bulk-boundary

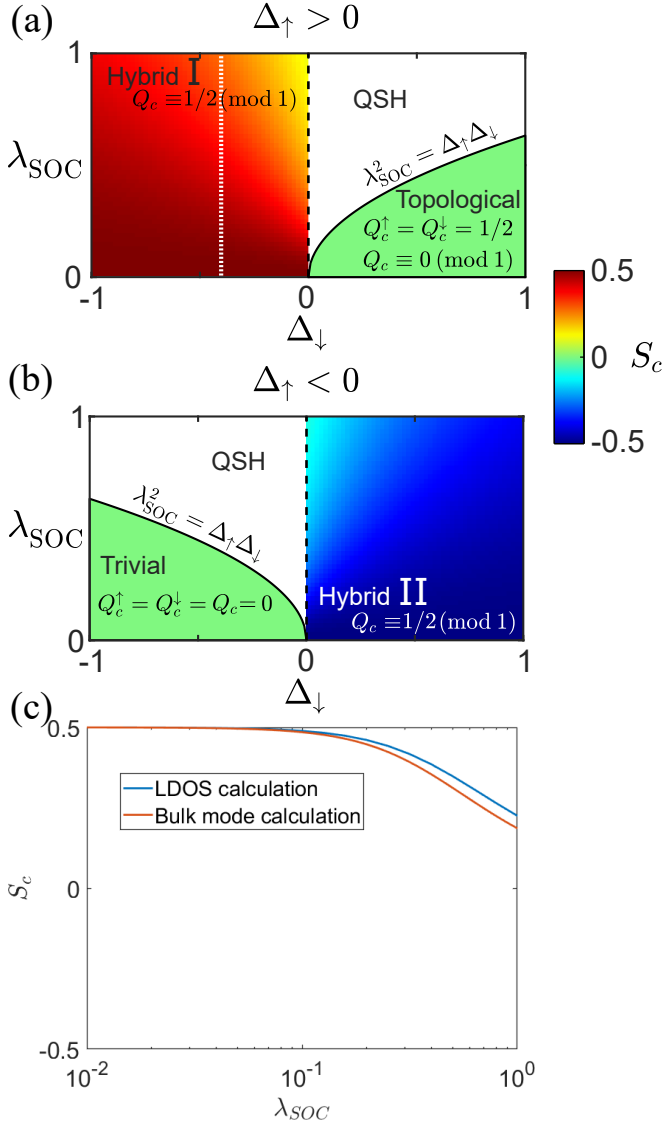


FIG. 1: Phase diagram of the Hamiltonian of Eq.(1). **(a)** $\Delta_\uparrow = 0.4$. Solid curve denotes phase transitions involving a bulk band gap closing and dashed black line denotes phase transition involving an edge band gap closing. The hybrid phase is marked by the Roman numeral I to distinguish it from the other hybrid phase in (b). QSH phase is marked in white. Color bar indicates the spin polarized corner charge values for the topological, trivial and hybrid phases. White dotted line marks $\Delta_\downarrow = -0.4$ used in sub figure (c). **(b)** $\Delta_\uparrow = -0.4$. **(c)** Comparison of S_c calculated according to Eq.(2) and LDOS corner calculation done at $\Delta_\uparrow = -\Delta_\downarrow = 0.4$.

correspondence principle (BBC) [33].

The two PhC designs shown in Fig.2(b) and (c) show such band inversion for both the independent TE-like and TM-like polarizations simultaneously. Fig.2(b) shows a PhC designed to have a trivial TE-like mode and a topological TM-like mode, while the PhC of Fig.2(c) was de-

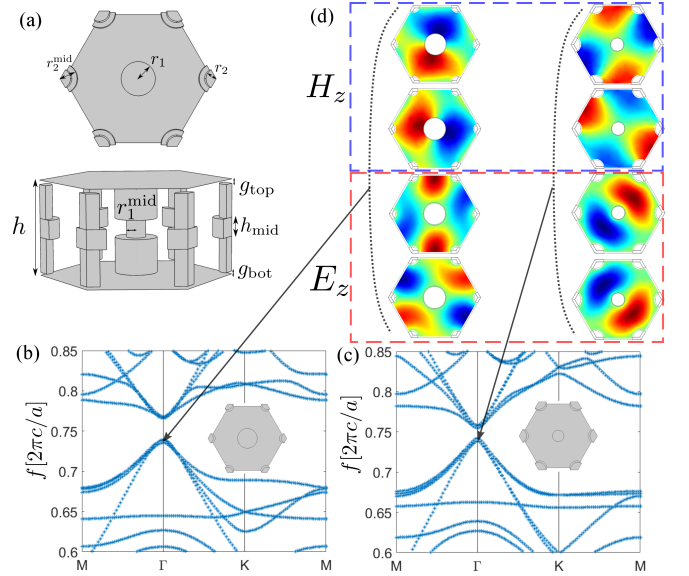


FIG. 2: Spin degenerate photonic topological insulator based on Kekulé distortion. **(a)** Top and side view of PhC unit cell. **(b)** Band structure for first hybrid phase. a is the magnitude of the primitive vectors of the unit cell. $r_1 = r_1^{\text{mid}} = 0.25a$, $r_2 = r_2^{\text{mid}} = 0.136a$, $g_{\text{top}} = g_{\text{bot}} = 0.045a$. **(c)** Band structure for second hybrid phase. $r_1 = r_1^{\text{mid}} = 0.147a$, $r_2 = r_2^{\text{mid}} = 0.191a$, $g_{\text{top}} = g_{\text{bot}} = 0.06a$. **(d)** Field profiles for the bands below the band gap at the Γ point for the structures of (b),(c). Dashed blue box for TE-like modes and dashed red box for TM-like modes. Arrows point to the band structure each field profile belongs to.

signed to have a topological TE-like mode and a trivial TM-like mode. Since the polarizations are orthogonal they each have their own corner charge, where the topological polarization has $Q_c^{\uparrow,\downarrow} = 1/2 \pmod{1}$ and the trivial has $Q_c^{\uparrow,\downarrow} = 0 \pmod{1}$. Both have $Q_c = 0 \pmod{1}$ but $S_c = +1/2$ for one phase and $-1/2$ for the other.

To introduce SOC in the PhCs one need only break the mirror symmetry by setting $g_{\text{top}} \neq g_{\text{bottom}}$ [23, 24]. We inspect the effect of SOC on the topological phase and hybrid phase in Fig.3(a),(c) and (b),(d) respectively, where for the topological phase the addition of SOC causes a Dirac cone to appear, while for the hybrid phase the effect of SOC is negligible. Further increase of the SOC term for the topological phase causes the band gap to reopen [10], indicating a topological phase transition. However, for the hybrid phases the addition of Kane-Mele SOC can never close the band gap. The reason for this difference is that the SOC only causes bands of the same orbital type to repel each other.

For the hybrid phases, we verify using a real space tight binding simulation and first principles simulations that corner modes exist at the zero energy at every 120° corner, as shown in Fig.4(a) and (b). We also verify

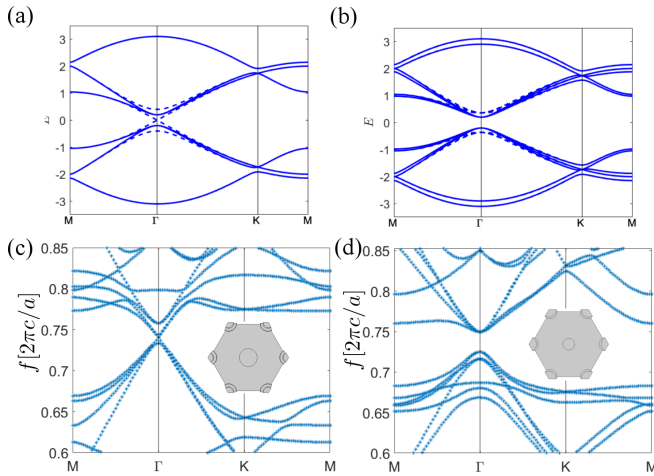


FIG. 3: Bulk band structures of topological and hybrid phases with and without SOC. **(a)** Bulk bands for $t_{in}^{\uparrow} = t_{in}^{\downarrow} = 0.8$, $t_{out}^{\uparrow} = t_{out}^{\downarrow} = 1.2$ and $t_{SOC} = 0$ in solid lines and with $t_{SOC} = 0.2$ in dashed lines. **(b)** For $t_{in}^{\uparrow} = t_{out}^{\uparrow} = 0.8$, $t_{out}^{\downarrow} = t_{in}^{\downarrow} = 1.2$. $t_{SOC} = 0$ for solid lines and $t_{SOC} = 0.2$ for dashed lines. **(c)** Topological phase with SOC strength tuned such that a Dirac cones appears at Γ . Parameters: $r_1 = 0.22a$, $r_1^{\text{mid}} = 0.08a$, $r_2 = 0.11a$, $r_2^{\text{mid}} = 0.21a$, $h_{\text{mid}} = 0.2a$, $g_{\text{bot}} = 0.02a$, $g_{\text{top}} = 0.08a$. **(d)** Hybrid phase with SOC. Parameters: Same as Fig.2(c) except for $g_{\text{top}} = 0.1a$.

that the addition of SOC to the hybrid phase does not affect the zero energy corner states (see supplementary). We used edge roughening [16] at the interface between domains to create a band gap between the edge modes to reveal the existence of the corner states.

For the topological phase interfacing the trivial phase we can see that in the absence of SOC we can still detect corner states at the mid-gap (Fig.5(a),(b)), but as SOC is added the bulk band gap closes, eventually reopening with no corner states (Fig.5(c),(d)). The addition of sufficient SOC causes a first and second order topological phase transition to a spin-Hall phase, but unlike previously known spin-Hall PhCs, Eq.(1) predicts that the Kekulé order is responsible for a folding of the K and K' valleys into the Γ point, resulting in the rearrangement of the topologically protected kink states from 1 per valley to 2 at the Γ point. This spin Hall phase is therefore expected to be a novel first order topological phase, distinct from our previous works' spin Hall phase [23, 24] since it has integer spin Chern numbers instead of half integer. Practically, this allows us to achieve topologically protected kink states without relying on an additional non-trivial PhC.

Since our results apply to any C_6 system with two DOFs coupled to each other with coupling that preserves C_2 and C_3 symmetries, one isn't limited to spinful condensed matter systems if they try to achieve one of the

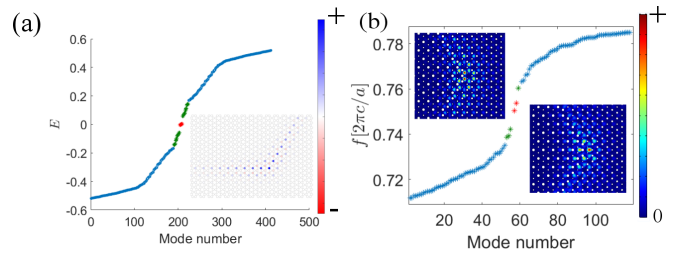


FIG. 4: Corner spectra for hybrid phases interfacing at 120° . **(a)** Eigenmodes for interface between two domains with $t_{in}^{\uparrow} = t_{out}^{\downarrow} = 1.2$, $t_{in}^{\downarrow} = t_{out}^{\uparrow} = 0.8$ for one domain, and $t_{in}^{\uparrow} = t_{out}^{\uparrow} = 0.8$, $t_{in}^{\downarrow} = t_{out}^{\downarrow} = 1.2$ for the other domain. Bulk modes in blue, kink modes in green, corner modes in red. Edge roughening factor is 2. Inset: corner mode profile, with color bar indicating mode amplitude. **(b)** First principles eigenmodes for interface between two hybrid phases with no SOC. Corner mode $|E|^2$ in top left insets and $|H|^2$ in the bottom right insets, with color bar marking the relative intensity. Left domain parameters are as in Fig.2(b) and right domain are as in Fig.2(c). Edge roughening used is $r_1^{\text{rough}} = 0.8r_1$, $r_2^{\text{rough}} = 1.2r_2$.

phases discussed in our letter. While the topological and trivial phases may be relatively straightforward to achieve using a spinful crystalline system, that is not the case for the hybrid phases, because the difference between spin-dependent hopping amplitudes is rather large. However, the hybrid phases may be more approachable by using bilayer graphene (BLG) where each layer has a different Kekulé texture.

Our designs open a new direction for active control of topological corner states, where active control of the mid-plane mirror symmetry can switch the topological corner states. For example, using the thermo-optical effect one can apply an external electromagnetic field to change the refractive index of some elements of the PhC [34], thereby breaking the mid-plane mirror symmetry, causing a topological phase transition to a spin-Hall phase. Furthermore, our work also shows how robustness to such symmetry breaking can be achieved to produce devices that are immune to that type of fabrication faults without compromising the number of protected corner states the device supports on each corner.

In summary, we've studied a hexagonal lattice tight binding model with spin dependent Kekulé textures, constructed a phase diagram showing three new C_6 HOTIs and one trivial C_6 insulator and realized it in a photonic crystal waveguide platform. We've also shown the different phases behave drastically different to the introduction of SOC. We've explained the origin of these differences and shown the effect on the topological corner modes using both an analytic model and first principles electromagnetic simulations. As part of our investigation

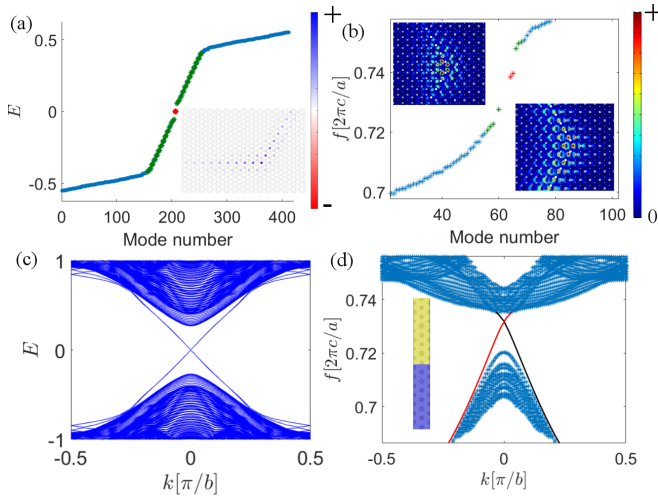


FIG. 5: Corner spectra for topological phase interfacing at 120° and kink spectra for QSH phase. **(a)** Modes for interface between two domains with $t_{\text{in}}^\uparrow = t_{\text{in}}^\downarrow = 1.2$, $t_{\text{out}}^\downarrow = t_{\text{out}}^\uparrow = 0.8$ for one domain, and $t_{\text{in}}^\uparrow = t_{\text{in}}^\downarrow = 0.8$, $t_{\text{out}}^\downarrow = t_{\text{out}}^\uparrow = 1.2$ for the other domain. **(b)** First principles eigenmodes for interface between topological phase and trivial phase. Corner mode $|E|^2$ in top left insets and $|H|^2$ in the bottom right insets, with color bar marking the relative intensity. Parameters for topological domain: $r_1 = 0.22a$, $r_1^{\text{mid}} = 0.08a$, $r_2 = 0.11a$, $r_2^{\text{mid}} = 0.21a$, $h_{\text{mid}} = 0.2a$, $g_{\text{top}} = g_{\text{bot}} = 0.02a$. Edge roughening used is $r_1^{\text{rough}} = 0.8r_1$, $r_2^{\text{rough}} = 1.2r_2$. **(c)** Kink spectrum of tight binding model between QSH phase and trivial phase. Hopping amplitudes are the same as in (a) and $\lambda_{\text{SOC}} = 0.4$ and $b = \text{sqrt}3a$ is the supercell periodicity. **(d)** Kink modes in red and black solid lines and bulk modes in blue asterisks. Inset: Top view of supercell structure. Topological domain with SOC is in blue and trivial domain in yellow. Parameters for topological domain: $r_1 = 0.22a$, $r_1^{\text{mid}} = 0.04a$, $r_2 = 0.132a$, $r_2^{\text{mid}} = 0.22a$, $h_{\text{mid}} = 0.2a$, $g_{\text{bot}} = 0.015a$, $g_{\text{top}} = 0.1a$. For trivial domain: $r_1 = 0.11a$, $r_1^{\text{mid}} = 0.04a$, $r_2 = 0.175a$, $r_2^{\text{mid}} = 0.1a$, $h_{\text{mid}} = 0.06a$, $g_{\text{bot}} = g_{\text{top}} = 0.045a$. Edge roughening used is $r_1^{\text{rough}} = 0.8r_1$, $r_2^{\text{rough}} = 1.2r_2$.

we've also described a new first order spin Hall photonic topological phase. Our results present an opportunity for future development of devices that allow the active switching of topological corner states.

* rag298@cornell.edu

- [1] F. D. M. Haldane, Physical review letters **61**, 2015 (1988).
 [2] C. L. Kane and E. J. Mele, Physical review letters **95**, 226801 (2005).

- [3] B. A. Bernevig and S.-C. Zhang, Physical review letters **96**, 106802 (2006).
 [4] T. Jungwirth, J. Wunderlich, and K. Olejnik, Nature materials **11**, 382 (2012).
 [5] T. Kimura, Y. Otani, T. Sato, S. Takahashi, and S. Maekawa, Physical review letters **98**, 156601 (2007).
 [6] X.-L. Qi, Y.-S. Wu, and S.-C. Zhang, Physical Review B **74**, 085308 (2006).
 [7] B. A. Bernevig, T. L. Hughes, and S.-C. Zhang, science **314**, 1757 (2006).
 [8] N. H. D. Khang, Y. Ueda, and P. N. Hai, Nature materials **17**, 808 (2018).
 [9] M. Jamali, J. S. Lee, J. S. Jeong, F. Mahfouzi, Y. Lv, Z. Zhao, B. K. Nikolić, K. A. Mkhoyan, N. Samarth, and J.-P. Wang, Nano letters **15**, 7126 (2015).
 [10] J. K. Asbóth, L. Oroszlány, and A. Pályi, Lecture notes in physics **919**, 997 (2016).
 [11] A. Kitaev, in *AIP conference proceedings*, Vol. 1134 (American Institute of Physics, 2009) pp. 22–30.
 [12] W. A. Benalcazar, B. A. Bernevig, and T. L. Hughes, Science **357**, 61 (2017).
 [13] F. Schindler, A. M. Cook, M. G. Vergniory, Z. Wang, S. S. Parkin, B. A. Bernevig, and T. Neupert, Science advances **4**, eaat0346 (2018).
 [14] C. W. Peterson, W. A. Benalcazar, T. L. Hughes, and G. Bahl, Nature **555**, 346 (2018).
 [15] B.-Y. Xie, H.-F. Wang, H.-X. Wang, X.-Y. Zhu, J.-H. Jiang, M.-H. Lu, and Y.-F. Chen, Physical Review B **98**, 205147 (2018).
 [16] M. Jung, R. G. Gladstone, and G. B. Shvets, Advanced Photonics **2**, 046003 (2020).
 [17] B.-Y. Xie, G.-X. Su, H.-F. Wang, H. Su, X.-P. Shen, P. Zhan, M.-H. Lu, Z.-L. Wang, and Y.-F. Chen, Physical review letters **122**, 233903 (2019).
 [18] X.-D. Chen, W.-M. Deng, F.-L. Shi, F.-L. Zhao, M. Chen, and J.-W. Dong, Physical Review Letters **122**, 233902 (2019).
 [19] Z. Qiao, W.-K. Tse, H. Jiang, Y. Yao, and Q. Niu, Physical review letters **107**, 256801 (2011).
 [20] M. J. Park, Y. Kim, G. Y. Cho, and S. Lee, Physical Review Letters **123**, 216803 (2019).
 [21] D. Pesin and A. H. MacDonald, Nature materials **11**, 409 (2012).
 [22] J. Lu, C. Qiu, W. Deng, X. Huang, F. Li, F. Zhang, S. Chen, and Z. Liu, Physical review letters **120**, 116802 (2018).
 [23] T. Ma, A. B. Khanikaev, S. H. Mousavi, and G. Shvets, Physical review letters **114**, 127401 (2015).
 [24] T. Ma and G. Shvets, Physical Review B **95**, 165102 (2017).
 [25] R. G. Gladstone, M. Jung, Y. Han, and G. Shvets, Physical Review B **100**, 245417 (2019).
 [26] W. A. Benalcazar, T. Li, and T. L. Hughes, Physical Review B **99**, 245151 (2019).
 [27] M. Ezawa, Physics Letters A **378**, 1180 (2014).
 [28] L.-H. Wu and X. Hu, Scientific reports **6**, 24347 (2016).
 [29] M. Ezawa, Physical Review B **97**, 155305 (2018).
 [30] C.-Y. Hou, C. Chamon, and C. Mudry, Physical review letters **98**, 186809 (2007).
 [31] J. D. Joannopoulos, S. G. Johnson, J. N. Winn, and R. D. Meade, Princeton Univ. Press, Princeton, NJ [ua] (2008).
 [32] L.-H. Wu and X. Hu, Physical review letters **114**, 223901 (2015).

- [33] R. S. Mong and V. Shivamoggi, *Physical Review B* **83**, 125109 (2011).
- [34] C. Sheng, H. Liu, S. Zhu, and D. A. Genov, *Scientific reports* **5**, 1 (2015).